

Size-scale effects in high-performance reinforced and prestressed concrete T-beams

*Original*

Size-scale effects in high-performance reinforced and prestressed concrete T-beams / Cafarelli, R.; Accornero, F.; Carpinteri, A.. - In: STRUCTURAL CONCRETE. - ISSN 1464-4177. - 24:5(2023). [10.1002/suco.202200673]

*Availability:*

This version is available at: 11583/2982315 since: 2023-09-19T14:50:49Z

*Publisher:*

John Wiley and Sons

*Published*

DOI:10.1002/suco.202200673

*Terms of use:*

This article is made available under terms and conditions as specified in the corresponding bibliographic description in the repository

*Publisher copyright*

(Article begins on next page)

## ARTICLE

# Size-scale effects in high-performance reinforced and prestressed concrete T-beams

Renato Cafarelli<sup>1</sup>  | Federico Accornero<sup>2</sup>  | Alberto Carpinteri<sup>1,3</sup>

<sup>1</sup>DISEG, Politecnico di Torino, Turin, Italy

<sup>2</sup>College of Engineering, Shantou University, Shantou, China

<sup>3</sup>Zhujiang (Pearl River) Professor of Guangdong Province, College of Engineering, Shantou University, Shantou, China

## Correspondence

Renato Cafarelli, DISEG, Politecnico di Torino, Turin, Italy.

Email: [renato.cafarelli@polito.it](mailto:renato.cafarelli@polito.it)

## Abstract

Reinforced concrete (RC) and prestressed concrete (PC) structural elements need to be designed in order to guarantee large plastic deformations, avoiding any loss in their load bearing capacity. In this framework, the rotation capacity of RC and PC beams has been demonstrated to be a function of concrete mechanical properties, reinforcement characteristics, and of the structural size. On the other hand, Theory of Plasticity as well as the International Standards completely disregard size-scale effects and ductile-to-brittle transitions, leading to an overlook of the strain-softening behavior of the concrete matrix and of the rotation capacity of RC beams. On the other hand, the Cohesive/Overlapping Crack Model is able to evaluate concrete cracking in tension and concrete crushing in compression, as well as snap-back and snap-through unstable phenomena, steel yielding and/or slippage. This Nonlinear Fracture Mechanics model predicts a reduction in the moment versus rotation plastic plateau by increasing the beam depth and/or the reinforcement percentage. The numerical investigations carried out on reinforced and prestressed high-performance concrete beams having rectangular or T-shaped cross-sections highlight the size-scale effects on plastic rotation capacity that allow to formulate new scale-dependent upper and lower limits of reinforcement percentage to guarantee a stable and ductile post-peak behavior of reinforced concrete structures.

## KEYWORDS

high-performance prestressed concrete, maximum reinforcement, minimum reinforcement, reinforced concrete, scale effects, T-beams

Discussion on this paper must be submitted within two months of the print publication. The discussion will then be published in print, along with the authors' closure, if any, approximately nine months after the print publication.

## 1 | INTRODUCTION

A comprehensive description of the flexural behavior of reinforced concrete (RC) structural elements must take into account the strain-softening and strain-localization of the concrete matrix, its different performances in tension and compression, and the mechanical instability

This is an open access article under the terms of the [Creative Commons Attribution-NonCommercial-NoDerivs](https://creativecommons.org/licenses/by-nc-nd/4.0/) License, which permits use and distribution in any medium, provided the original work is properly cited, the use is non-commercial and no modifications or adaptations are made.

© 2023 The Authors. Structural Concrete published by John Wiley & Sons Ltd on behalf of International Federation for Structural Concrete

phenomena occurring in the loading process, such as concrete cracking in tension, reinforcement yielding, and concrete crushing in compression. Typical load-deflection diagrams can be characterized in their early stages by an elastic regime up to the first cracking load,  $P_{cr}$ , followed by a virtual unstable branch along which there is a decrease in both external load,  $P$ , and deflection,  $\delta$ . This branch is commonly neglected during laboratory tests, since a snap-through behavior, with a sudden increase in deflection, or a snap-back instability, with a catastrophic loss in bearing capacity, is registered. More generally, evidences of snap-back and snap-through instabilities may appear in the response of thin cylindrical shells under axial compression as outlined by von Kármán and Tsien,<sup>1</sup> and in the response of complete spherical shells and spherical caps subjected to external pressure, as highlighted by Carlson et al.<sup>2</sup> and Kaplan.<sup>3</sup> Snap-through local instabilities are often observed in the case of composite materials such as reinforced concrete and fiber-reinforced mortar, due to the fact that the reinforcements act as crack arresters, producing a global ductile response as observed by Zhu and Bartos.<sup>4</sup>

In this framework, effective interpretations of such instability phenomena have been proposed by means of the Bridged Crack Model<sup>5-7</sup> highlighting the crucial role of a nondimensional parameter called *reinforcement brittleness number*,  $N_P$ , governing the ductile versus brittle response of the structural element. On the other hand, analytical and numerical investigations carried out by means of the Cohesive Crack Model on plain concrete specimens<sup>8-10</sup> evidenced another nondimensional parameter, the *matrix brittleness number*,  $s_E$ , which is able to capture the transition from stable to unstable behavior either by increasing the specimen size, and/or the material tensile strength,  $\sigma_t$ , and/or by decreasing the fracture energy,  $G_F$ . As a matter of fact, modern design approaches require that RC structures present a sufficient deformation capacity<sup>11</sup> for warning before failure, the possibility of moment redistribution in the case of statically indeterminate structures, the ability to react to accidental loadings (robustness), together with energy dissipation in case of earthquake and fire resistance. In this framework, the nonlinear behavior of RC beams has been demonstrated<sup>12</sup> to be dependent on mechanical, geometrical, and loading characteristics, suggesting that simplified models<sup>13</sup> are inadequate to predict plastic resources of real structures. Different numerical and experimental investigations<sup>14</sup> have demonstrated that a decrease in plastic rotation capacity becomes manifest by increasing the reinforcement ratio,  $\rho$ , and/or by increasing the beam depth.<sup>15-18</sup>

Several models have been proposed to predict RC plastic rotation capacity, among which we can mention the Hillerborg Model,<sup>19</sup> the Naples Model,<sup>20,21</sup> and the Delft Model,<sup>22,23</sup> among others. In the present paper, the

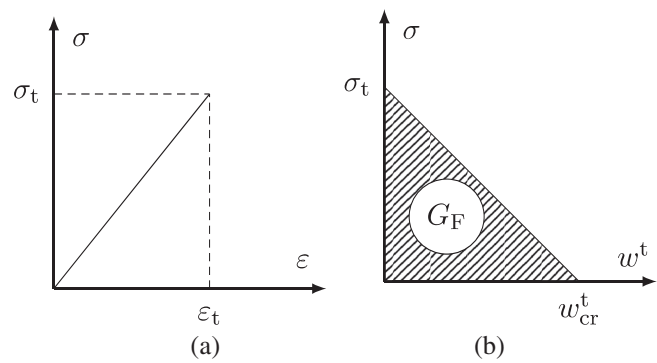


**FIGURE 1** Cohesive Crack Model for concrete: (a) Linear elastic stress-strain law in tension; (b) Postpeak  $\sigma$ - $w^t$  cohesive relationship.

Cohesive/Overlapping Crack Model<sup>24</sup> together with a Dimensional Analysis<sup>25,26</sup> approach are used to investigate the effects of beam depth and cross-section shape, concrete grade, as well as reinforcement percentage on the plastic rotation capacity of RC beams.

The Cohesive Crack Model<sup>9,10</sup> is able to describe the damage evolution in the tension zone of a concrete cross-section subjected to bending, assuming a linear elastic constitutive law (Figure 1a) up to the first peak load, and a constitutive law in the form  $\sigma$ - $w^t$ , being  $\sigma$  the applied stress and  $w^t$  the crack opening displacement, in the zone where strain localization in tension occurs. More precisely, within the Cohesive Crack Model, a fictitious crack,<sup>27,28</sup> longer than the real one, is introduced, providing a damage process zone where the material is still able to transfer tensile closing forces, albeit partially damaged. Thus, the residual bearing capacity of the structural element is simulated by means of the application of closing forces along the crack faces according to the constitutive law of Figure 1b, where  $w^t_{cr}$  is the threshold value of crack opening beyond which the closing forces vanish. The area subtended by the  $\sigma$ - $w^t$  diagram represents the fracture energy of the concrete matrix,  $G_F$ , that can be determined according to Model Code 2010<sup>29</sup> as:

$$G_F = 0.073(\sigma_c + 8)^{0.18} \quad (1)$$

$\sigma_c$  being the concrete compression strength. The Cohesive Crack Model has been effectively applied in the study of plain concrete or lightly reinforced/high-strength concrete beams, not considering the potential crushing failure occurring in the compression zone of RC beam cross-sections.<sup>27,28,30,31</sup>

The constitutive law currently adopted in Model Code 2010<sup>29</sup> for concrete in compression is based on the experimental and numerical investigations carried out by Hognestad,<sup>32</sup> Popovic<sup>33</sup> and Meyer<sup>34</sup>:

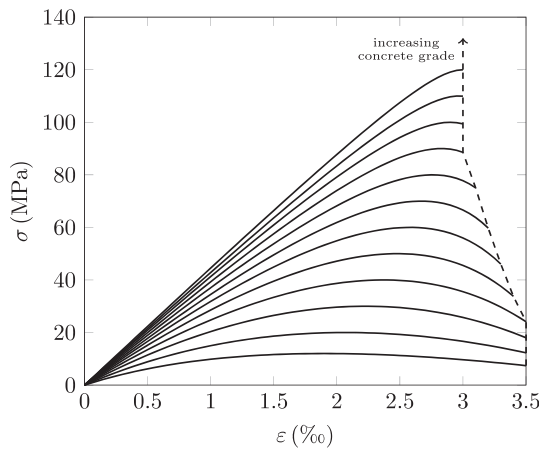


**FIGURE 2** Stress-strain curves for different concrete grades (adapted from *fib* Model Code 2010).<sup>29</sup>

$$\sigma = -\sigma_c \frac{k\eta - \eta^2}{1 + (k-2)\eta} \quad (2)$$

$k$  and  $\eta$  being parameters that are functions of the concrete strength. Equation (2) is represented in Figure 2 for concrete grades between C12 and C120, suggesting that this constitutive law is not able to thoroughly predict the ductile-to-brittle transition occurring for high-performance concrete (HPC) since in the postpeak regime the variation from a negative (softening) to a positive (snap-back) slope by increasing the concrete strength is not captured.<sup>35,36</sup> As a matter of fact, recent experimental investigations pointed out that postpeak stress-strain relationships are highly influenced by testing conditions, specimen shape, and specimen slenderness.<sup>37–39</sup> In this framework, the Round Robin<sup>40</sup> organized by RILEM in 1997 outlined that, in order to effectively take into account the strain localization of concrete in compression, an effective constitutive law in the postpeak regime must be identified in a  $\sigma$ - $w^c$  diagram, being  $w^c$  an inelastic displacement, rather than in a classic  $\sigma$ - $\varepsilon$  diagram. The experimental investigations carried out by RILEM leads to the definition of the crushing energy,  $G_c$ , and several experimental campaigns<sup>41–43</sup> have been carried out to assess this parameter for both normal-strength concrete (NSC) and HPC. Moreover, constitutive models based on a Fracture Mechanics approach have proved to be capable of thoroughly predict the damaging process of concrete in compression.<sup>44,45</sup>

In this framework, Carpinteri and co-workers<sup>45</sup> introduced the Overlapping Crack Model, which is able to describe the crushing damage of concrete through a fictitious interpenetration zone developing in the region where compressive strain localization takes place. The parameters involved in the Overlapping Crack Model are formally similar to those of the Cohesive Crack Model. The main

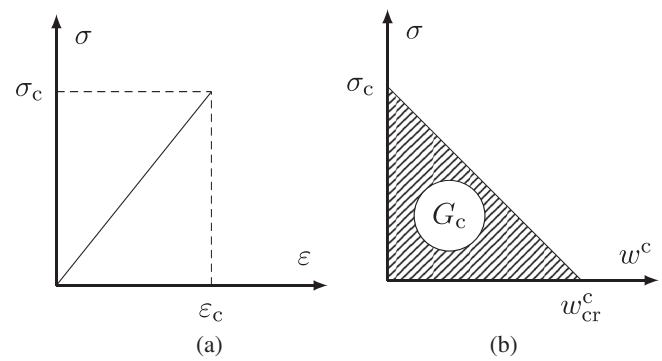


**FIGURE 3** Overlapping Crack Model for concrete: (a) Linear elastic stress-strain law in compression; (b) Post-peak stress versus fictitious interpenetration relationship.

variables entailed within this model are: the concrete compression strength,  $\sigma_c$ , the threshold value of fictitious interpenetration beyond which the virtual opening compressive forces vanish,  $w^c_{cr}$ , and the crushing energy of concrete,  $G_c$ , which can be calculated as the area subtended by the  $\sigma$ - $w^c$  diagram of Figure 3b. In this framework, Suzuki et al.<sup>46</sup> carried out an experimental campaign on RC columns and proposed the following relationship for  $G_c$ :

$$G_c = 80 - 50k, \quad (3)$$

being  $k = 40/\sigma_c \leq 1$ . According to the Overlapping Crack Model, the material behaves elastically until the concrete compression strength,  $\sigma_c$ , is reached (Figure 3a); then a constitutive law in the form  $\sigma$ - $w^c$  (Figure 3b) is adopted.

Therefore, the Cohesive/Overlapping Crack Model (COCM)<sup>24,47</sup> is able to describe by means of the two above-mentioned constitutive laws the whole structural behavior of RC elements subjected to bending, considering local and global discontinuous phenomena within the damage process: in particular, cracking and crushing instabilities are proved to set the minimum and maximum reinforcement percentages,  $\rho_{min}$  and  $\rho_{max}$ , for RC beams.<sup>24,48,49</sup>

In this sense, despite several studies have proposed an equivalent stress block for non-rectangular<sup>50–52</sup> and high-strength<sup>53</sup> concrete beams, a comprehensive and effective study of size-scale effects on the rotation capacity of RC T-beams is still lacking.

In the present paper, COCM is adopted to analyze the ductile-to-brittle size-scale transition in high-performance reinforced (HPRC) or prestressed concrete (HPPC) T-beams. For RC beams, this model is able to point out how the scale-dependent reinforcement limits,  $\rho_{min}$  and  $\rho_{max}$ , between which RC structures present a stable behavior without catastrophic losses in their bearing capacity due to concrete cracking (hyperstrength) or crushing, are functions of the beam cross-section shape. On the other hand, the application of the Cohesive/Overlapping Crack Model to HPPC T-beams

clearly highlights their brittleness at the Ultimate Limit State (ULS) due to the presence of the prestressing force and of the high concrete strength, demonstrating how an effective and rational maximum reinforcement ratio can represent a strict requirement for these structural elements.

## 2 | THE COHESIVE/OVERLAPPING CRACK MODEL (COCM)

COCM considers a beam cross-section divided into  $n$  nodes, simulating the propagation of the cohesive and the overlapping process zones by means of a step-by-step procedure. More in detail, by means of the superposition principle, it is possible to write:

$$\{w\} = [K_F]\{F\} + [K_F]\{F_p\} + \{K_M\}M, \quad (4)$$

where  $\{w\}$  is the vector containing the opening/overlapping displacements;  $[K_F]$  is the matrix containing the nodal displacements generated by unit nodal forces;  $\{F\}$  is the vector containing the nodal forces;  $\{F_p\}$  is the vector containing the nodal forces generated by a possible prestressing force;  $\{K_M\}$  is the vector containing the nodal displacements generated by a unit bending moment, and  $M$  is the value of the applied bending moment (Figure 4). The unknowns involved in Equation (4) are  $(2n + 1)$ , namely,  $\{w\}$ ,  $\{F\}$ , and  $M$ . At each step, the cohesive or the overlapping process zone advances, and, in the general case of Figure 4, the following conditions are applied:

$$F_i = 0 \quad \text{for } i = 1, \dots, (j-1), i \neq r \quad (5a)$$

$$F_i = F_t \left(1 - \frac{w_i}{w_{cr}^t}\right) \quad \text{for } i = j, \dots, (m-1) \quad (5b)$$

$$w_i = 0 \quad \text{for } i = m, \dots, p \quad (5c)$$

$$F_i = F_c \left(1 - \frac{w_i}{w_{cr}^c}\right) \quad \text{for } i = (p+1), \dots, q \quad (5d)$$

$$F_i = 0 \quad \text{for } i = (q+1), \dots, n \quad (5e)$$

$$F_i = f(w_i) \quad \text{for } i = r \quad (5f)$$

where  $j$  is the real cohesive crack tip;  $m$  is the fictitious cohesive crack tip;  $p$  is the fictitious overlapping zone tip;  $q$  is the real overlapping zone tip.

Equation (5f) expresses the bridging force,<sup>5,6</sup>  $F_b$ , exerted on crack faces due to the presence of a reinforcement layer. The bridging action includes the cohesive forces of the concrete matrix, the tensile stiffness of the bar, and the hardening effect due to the interaction between concrete and the reinforcement layer (the so-called “tension stiffening” effect).<sup>54</sup> In the present paper, the first contribution is acknowledged automatically by means of the application of Equation (4). On the other hand, the contributions of the bar and the hardening effect are assessed by means of the equilibrium procedure reported in Ruiz et al.<sup>30</sup> and Accornero et al.,<sup>55</sup> leading to the definition of the following constitutive law:

$$F_b = \sqrt{\pi \phi \tau_m E_s A_s w^t} \quad \text{for } w^t < w_y^t \quad (6a)$$

$$F_b = F_y - F_p \quad \text{for } w^t \geq w_y^t \quad (6b)$$

$\phi$  being the bar diameter,  $\tau_m$  the average shear stress at steel-concrete interface,  $E_s$  the steel Young's modulus,  $A_s$  the steel-bar area,  $F_y$  the steel yielding force, and  $w_y^t$  the crack opening displacement corresponding to steel-bar yielding. In Figure 5, the nonlinear bridging condition of Equation<sup>6</sup> is reported. In this framework, the development length,  $\ell_d$ , which is required to generate steel yielding is:

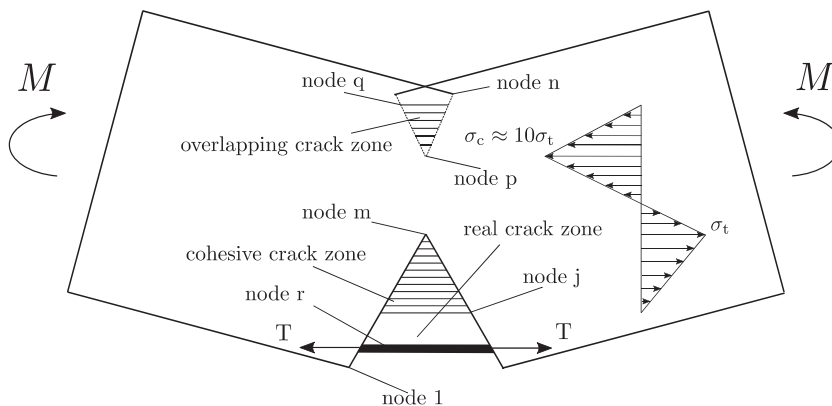
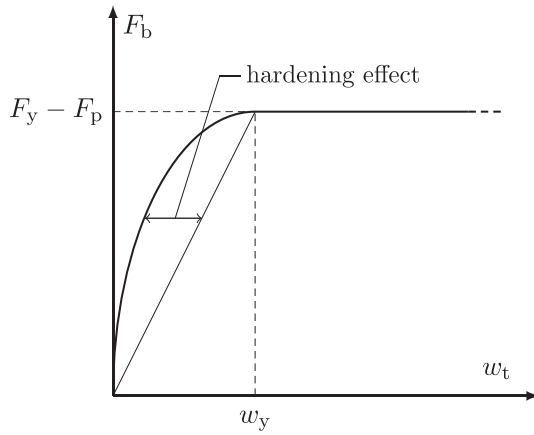


FIGURE 4 Cohesive/Overlapping Crack Model (COCM).



**FIGURE 5** Bridging force exerted by reinforcement on crack faces.

$$\ell_d = \frac{F_y - F_p}{\pi \phi \tau_m} \quad (7)$$

When the real development length depending on beam geometry,  $\ell_{d,\max}$ , is smaller than  $\ell_d$ , the reinforcement slip occurs at a constant bridging force,  $F_{b,s}$ :

$$F_{b,s} = \frac{(F_y - F_p) \ell_{d,\max}}{\ell_d} \quad (8)$$

Equations (5) reduce the unknowns of Equation (4) but do not permit the calculation of the bending moment,  $M$ . In this framework, a Crack Length Control Scheme solution technique coupled with a modified Newton-Raphson method is adopted and for each calculation step,  $M$  is fixed according to the minimum value of the external load that generates the ultimate tensile force,  $F_t$ , at the fictitious opening tip or the ultimate compressive force,  $F_c$ , at the fictitious overlapping tip. Only the tip that reaches the ultimate condition for the considered step is moved, allowing the cohesive or the overlapping process zone to extend. At the end of each calculation step, the rotation angle is computed exploiting Betti's Theorem:

$$\vartheta = \{K_M\}^T \{F\} + D_M M \quad (9)$$

$D_M$  being the rotation generated by a unit bending moment.

The numerical procedure presented above permits the calculation of the nonlinear response of the beam section in the  $M - \vartheta$  diagram. On the other hand, the structural response can be obtained in the  $P - \delta$  diagram following the procedure proposed by Mattock.<sup>15</sup> In this framework, the mid-span deflection,  $\delta$ , can be regarded as the sum of two contributions (Figure 6): a displacement due to local rotation,  $\delta_f$ , and a second contribution

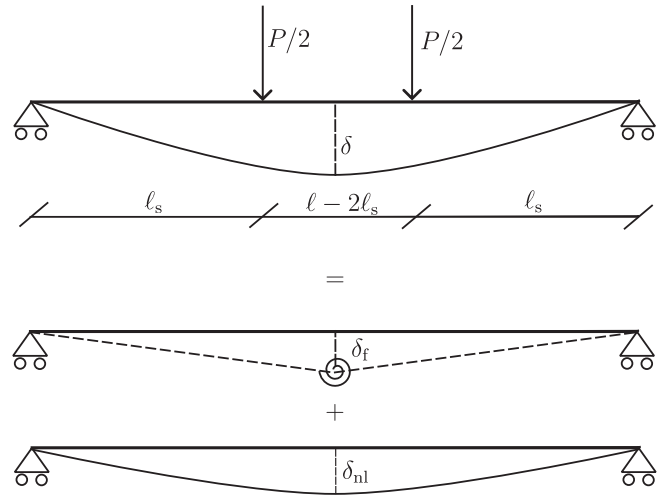


**FIGURE 6** Superposition principle for the structural response of the damaged beam.

due to the nonlinear behavior of the concrete matrix along the beam span,  $\delta_{nl}$ :

$$\delta = \delta_f + \delta_{nl} \quad (10)$$

Referring to Figure 6,  $\delta_f$  can be computed as:

$$\delta_f = \frac{\vartheta \ell}{4} \quad (11)$$

On the other hand, we have:

$$\delta_{nl} = \frac{1}{8} \frac{M \ell^2}{EI_e} - \frac{1}{6} \frac{M \ell_s^2}{EI_e} \quad (12)$$

$I_e$  being the equivalent inertia of the beam<sup>56</sup> and  $\ell_s$  the beam shear span.  $I_e$  takes into account multiple crack formation and propagation along the beam span and it can be assessed following the procedure proposed by ACI 318-19<sup>57</sup> and ACI RC Design Handbook.<sup>58</sup> Moreover, the load,  $P$ , acting on the beam can be computed as (Figure 6):

$$P = \frac{2M}{\ell_s} \quad (13)$$

Then, when the  $M - \vartheta$  curve is obtained, the  $P - \delta$  diagram can be calculated by means of Equations (10–13).

### 3 | PARAMETRIC ANALYSES

A numerical study on the flexural behavior of RC beams is reported in Figure 7. The parametric analysis has been performed on six beam depths,  $h$ , assuming for the

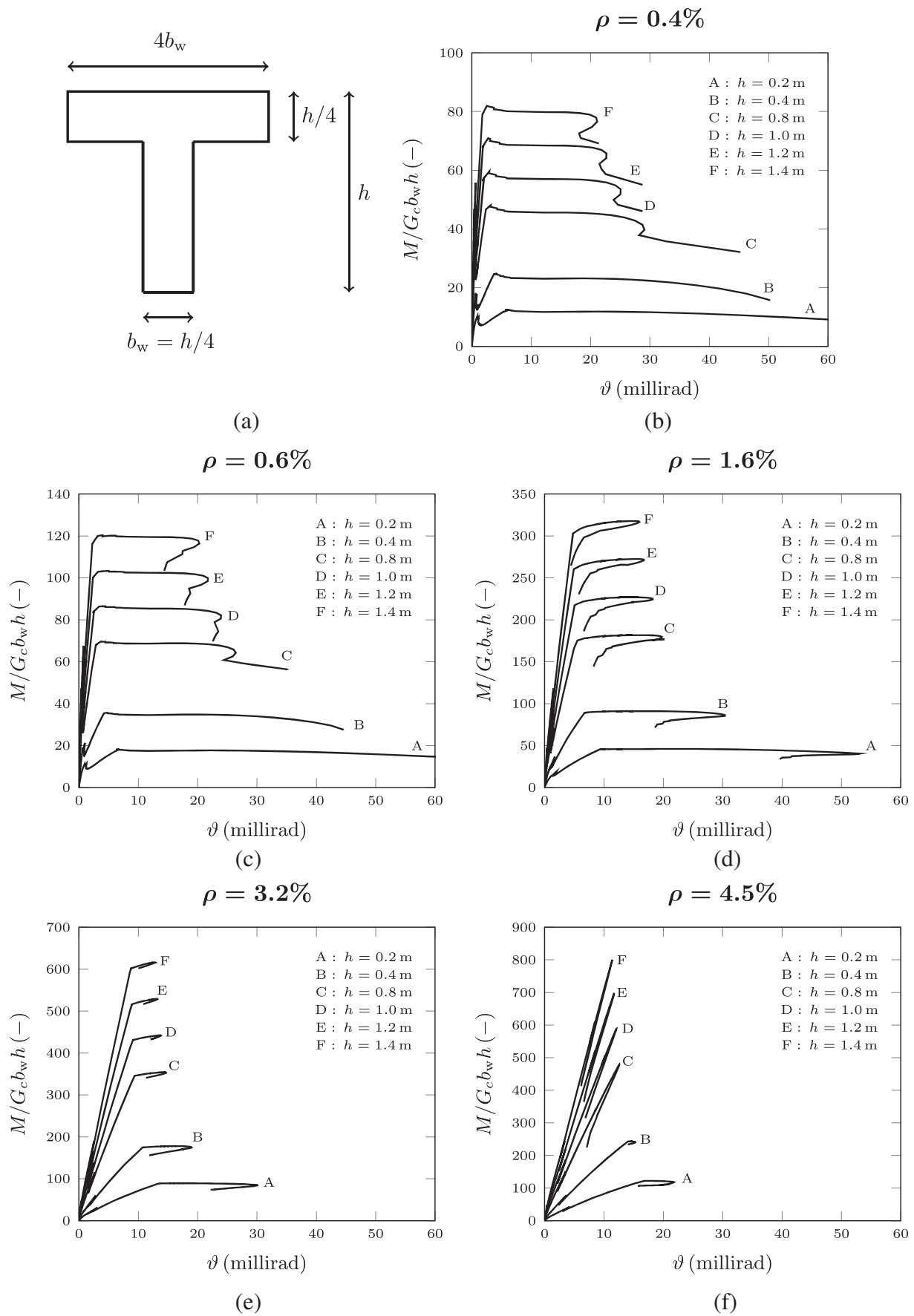


**FIGURE 7** Nondimensional load versus rotation curves for RC T-beams: (a) beam cross- section; (b)  $\rho = 0.4\%$ ; (c)  $\rho = 0.6\%$ ; (d)  $\rho = 1.6\%$ ; (e)  $\rho = 3.2\%$ ; (f)  $\rho = 4.5\%$ .



concrete matrix a tensile strength  $\sigma_t = 4$  MPa, a compression strength  $\sigma_c = 40$  MPa, a fracture energy,  $G_F$ , and a crushing energy,  $G_c$ , equal to 0.15 N/mm and 30 N/mm according to Equation (1) and Equation (3), respectively. Steel reinforcement has been assumed to have a yield strength,  $\sigma_y$ , equal to 500 MPa, and its position is fixed in order to keep the ratio between the effective depth of the beam and the overall depth,  $d/h$ , equal to 0.9. All the investigated beams have a web thickness,  $b_w$ , and a flange thickness equal to  $h/4$  with a flange width of  $4b_w$  as reported in Figure 7a. The beam depth,  $h$ , varies between 0.2 m and 1.4 m in order to highlight size-scale effects.

In Figure 7b, different structural behaviors are obtained assuming  $\rho = 0.4\%$ . Here, the beam having  $h = 0.2$  m exhibits a large rotational capacity with a wide

plastic plateau after steel yielding. Increasing the beam depth, plastic resources decrease, and early brittle crushing failure is registered. In Figure 7c, with  $\rho = 0.6\%$ , it is possible to observe a large reduction in plastic rotation capacity, and an even more important role played by the ultimate compressive behavior of the concrete matrix. The ductile-to-brittle transition is evident comparing Figure 7d,e, where  $\rho = 1.6\%$  and  $\rho = 3.2\%$  are considered. Due to the higher reinforcement ratio, the extension of the plastic plateau is reduced, and a snap-back due to crushing is present at the end of each horizontal branch for the whole beam depth range. In Figure 7f the curves C to F ( $0.8 \text{ m} < h < 1.4 \text{ m}$ ) exhibit the most brittle behavior, since, once the peak load has been reached, a sudden loading drop is registered due to the unstable growth of the overlapping process zone without steel yielding. For

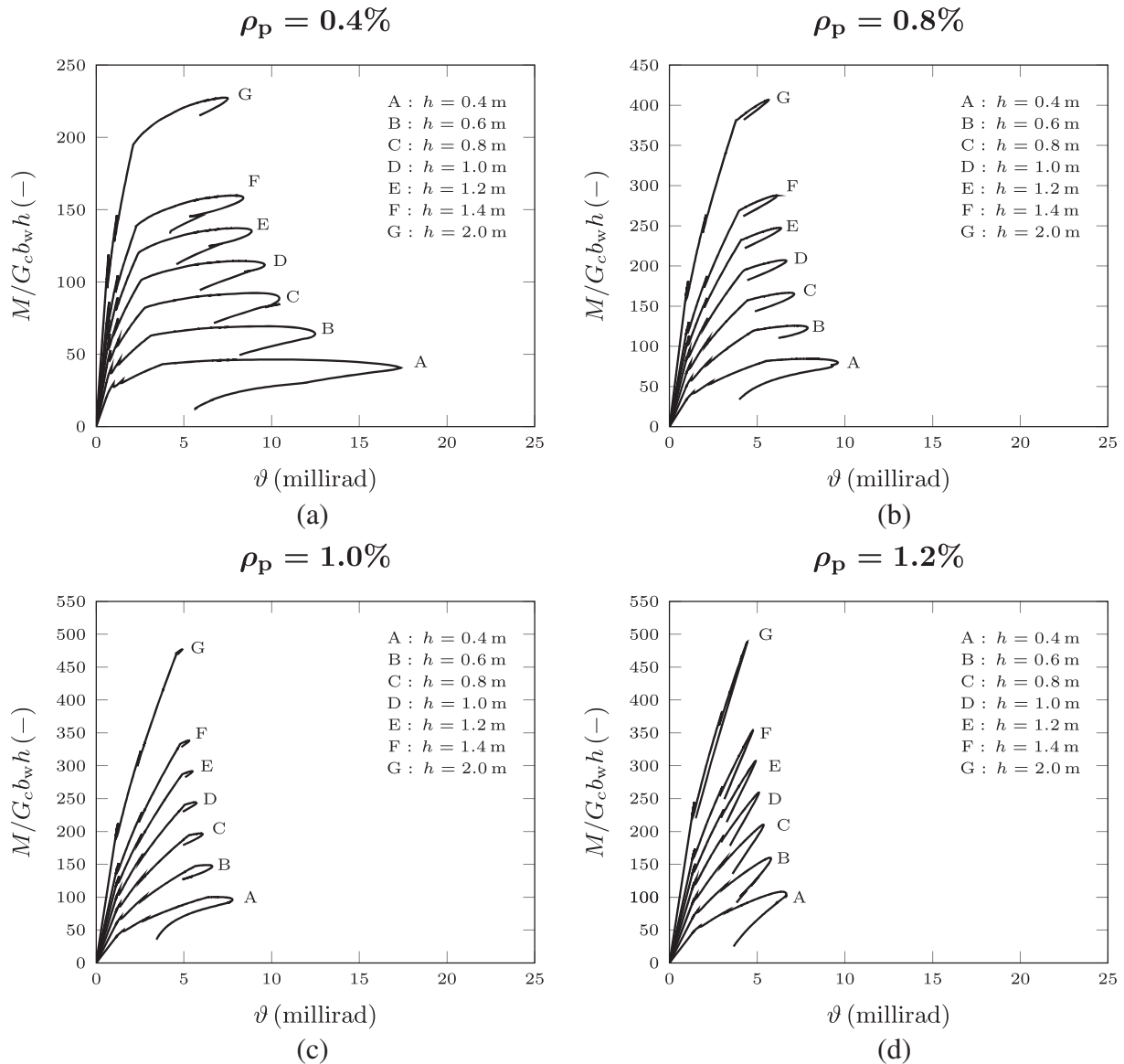


FIGURE 8 Nondimensional load versus rotation curves for PC T-beams: (a)  $\rho_p = 0.4\%$ ; (b)  $\rho_p = 0.8\%$ ; (c)  $\rho_p = 1.0\%$ ; (d)  $\rho_p = 1.2\%$ .



this high-steel percentage, only beams with  $h = 0.2$  m and  $h = 0.4$  m exhibit steel yielding.

In Figure 8 a parametric analysis of the structural behavior of PC T-beams subjected to bending is reported. Within the Cohesive/Overlapping Crack Model, PC beams casted with pretensioning technique or, more generally, having a straight steel strand layout can be taken into consideration. In these simulations, the concrete matrix presents the same mechanical properties as in the previous study on RC beams, the prestressing force is equal to  $2/3 A_{sp} \sigma_y$ , being  $A_{sp}$  the prestressing steel area, and  $\sigma_y = 1700$  MPa the steel yield strength. The analysis is performed on beams having a flange width of  $2b_w$  with a thickness of  $h/4$ . In Figure 8a, where  $\rho_p = 0.4\%$ , it is possible to observe a first elastic branch up to the cracking load, a first descending branch due to cracking (snap-back) instability, a second ascending branch due to the steel strand activation, and a plastic plateau involving steel yielding.

At the end of each plastic plateau, a catastrophic snap-back due to concrete crushing is observed. As for RC beams, the extension of the plastic plateau decreases as reinforcement percentage and/or beam depth increases, albeit lower plastic rotations are evidenced due to the presence of the prestressing force (Figure 8a,b). The increase in the reinforcement ratio,  $\rho_p$ , beyond  $0.8\%$ , reduces the global ductility as may be observed in Figure 8c, where the beam having  $h = 2.0$  m presents an almost balanced reinforcement condition with a small plastic plateau. In Figure 8d, all the curves present an unstable behavior governed by brittle concrete crushing without steel yielding.

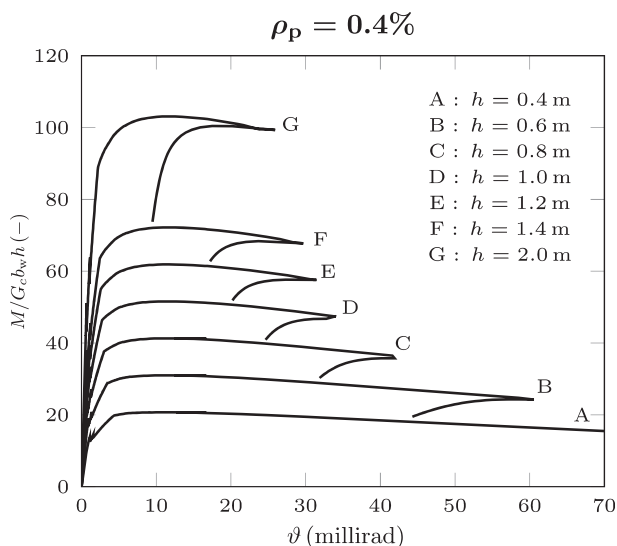


FIGURE 9 Nondimensional load versus rotation curves for HPPC T-beams ( $\rho_p = 0.4\%$ ).

In Figure 9, a parametric analysis of the structural behavior of HPPC T-beams is reported. In this study the concrete matrix presents a compression strength  $\sigma_c = 150$  MPa, a tension strength  $\sigma_t = 6$  MPa, a fracture energy,  $G_F$ , and a crushing energy,  $G_c$ , equal to  $0.18$  N/mm (Equation (1)) and  $70$  N/mm (Equation (3)), respectively. The beams present the same geometry and the same prestressing force as the previous analysis and a steel percentage of  $\rho_p = 0.4\%$  is considered. In this case, due to the high strength of the concrete matrix, wider plastic plateaus as well as more brittle behaviors of the post-crushing regime are detected.

#### 4 | NUMERICAL VERSUS EXPERIMENTAL COMPARISON

In the following, a numerical versus experimental comparison is proposed to investigate the scale effects on the structural behavior of HPRC beams. The experimental campaign carried out by Ashour<sup>59</sup> on beams cast with three different concrete grades (see Table 1) is discussed. The concrete tension strength,  $\sigma_t$ , and the fracture energy,  $G_F$ , are estimated according to Model Code<sup>29</sup> and Equation (1), respectively. On the other hand, the crushing energy,  $G_c$ , is calculated by means of Equation (3). The beams have a cross section of  $200 \times 250$  mm and are tested up to failure by means of a four point bending loading scheme as reported in Figure 10.

In Figure 11, the numerical (thick curve) versus experimental (thin curve) comparison is reported. It is possible to observe that COCM is able to thoroughly describe the post-cracking non-linear behavior of the beams and their ductile-to-brittle transition by increasing the reinforcement ratio,  $\rho$ . In the case of HPRC beams (H series), COCM is able to predict the increase in the plastic rotational capacity due to the increase in the concrete matrix strength. Finally, it is worth noting that snap-back phenomena can be detected during experimental testing only if an increasing function of time, such as the crack mouth opening displacement (CMOD), is used as controlling parameter. In this case, the experimental campaign carried out by Ashour was unable to follow snap-back branches in a stable manner since a load controlling technique was adopted.

#### 5 | MINIMUM AND MAXIMUM REINFORCEMENT PERCENTAGES FOR RC BEAMS

The numerical simulations reported in Figures 7, 8 and 9 outline the existence of a scale-dependent maximum

**TABLE 1** Mechanical properties of the beams tested by Ashour<sup>59</sup>

Beam No.	$\rho$ (%)	$\sigma_c$ (MPa)	$\sigma_t$ (MPa)	$G_F$ (N/mm)	$G_c$ (N/mm)
B-N2	1.18	48.6	4.0	0.151	38.856
B-N3	1.77	48.6	4.0	0.151	38.856
B-N4	2.37	48.6	4.0	0.151	38.856
B-M2	1.18	78.5	4.8	0.163	54.522
B-M3	1.77	78.5	4.8	0.163	54.522
B-M4	2.37	78.5	4.8	0.163	54.522
B-H2	1.18	102.4	5.3	0.170	60.469
B-H3	1.77	102.4	5.3	0.170	60.469
B-H4	2.37	102.4	5.3	0.170	60.469

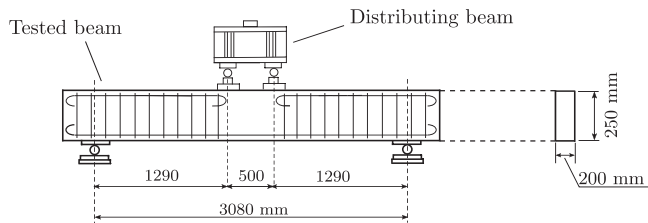


**FIGURE 10** Testing set-up and beam geometry adopted by Ashour.<sup>59</sup>

reinforcement ratio,  $\rho_{\max}$ , beyond which the concrete crushing failure occurs prior to steel yielding. Currently, an effective scale-dependent minimum reinforcement ratio,  $\rho_{\min}$ , proposed by Carpinteri and co-workers<sup>24</sup> has been acknowledged by the American Association of State Highway Transportation Officials (AASHTO)<sup>60</sup> in order to avoid the scale-dependent hyperstrength behavior due to cracking instability. On the other hand, all the international provisions about maximum reinforcement percentage may lead to unsafe and costly structural design, since the traditional constitutive laws adopted to obtain those Standards are not able to predict the brittleness of the concrete matrix. In this framework, only an effective dimensional analysis<sup>26</sup> approach is able to clearly outline the main variables involved in the problem of determining minimum and maximum reinforcement percentages for RC T-beams.

More specifically, the variables involved in the flexural behavior of RC beams may be written as<sup>24</sup>:

$$M = F(\sigma_t, G_F, \sigma_c, G_c, E, \sigma_y, \rho, h; b_w/h, b/h, \ell/h; \vartheta) \quad (14)$$

being  $\ell$  the beam span and  $E$  the concrete Young's modulus. Note that, if we were interested in lightly reinforced concrete beams, the two variables  $\sigma_c$  and  $G_c$  could be neglected since beams having a low reinforcement ratio exhibit at the ULS the steel yielding rather than the concrete crushing. Thus, assuming the beam depth,  $h$ , and

the fracture toughness,  $K_{IC} = (G_F E)^{0.5}$  as independent variables, Equation (14) leads to:

$$\frac{M}{K_{IC} h^{2.5}} = \Pi \left( \frac{K_{IC}}{\sigma_t h^{0.5}}, \rho \frac{\sigma_y h^{0.5}}{K_{IC}}, \vartheta \frac{K_{IC}}{E h^{0.5}} \right) \quad (15)$$

where it is possible to recognize the matrix brittleness number  $s_t = K_{IC}/(\sigma_t h^{0.5})$ , and the reinforcement brittleness number  $N_P^L = \rho \sigma_y h^{0.5}/K_{IC}$  introduced by Carpinteri<sup>5</sup> as governing parameters. On the other hand, if we are interested in the investigation of heavily reinforced beams, we may neglect  $\sigma_t$  and  $G_F$  in Equation (14), since for large reinforcement percentages the concrete crushing precedes steel yielding.<sup>31</sup> Thus, assuming  $h$  and  $(G_c E)^{0.5}$  as new fundamental variables, Equation (14) may be rewritten as:

$$\frac{M}{\sqrt{G_c E} h^{2.5}} = \Pi \left( \frac{\sqrt{G_c E}}{\sigma_c h^{0.5}}, \rho \frac{\sigma_y h^{0.5}}{\sqrt{G_c E}}, \vartheta \frac{\sqrt{G_c E}}{E h^{0.5}} \right) \quad (16)$$

where it is possible to recognize the matrix brittleness number,  $s_c = (G_c E)^{0.5}/\sigma_c h^{0.5}$ , and the reinforcement brittleness number,  $N_P^U = \rho \sigma_y h^{0.5}/(G_c E)^{0.5}$ .

A parametric analysis of RC T-beams subjected to bending can be realized by means of COCM in order to outline  $\rho_{\min}$  and  $\rho_{\max}$  trends in the planes  $s_t - N_P^L$  and  $s_c - N_P^U$ , respectively. This analysis considers the concrete matrix characterized by a compression strength,  $\sigma_c$ , varying between 20 and 80 MPa, the tension strength,  $\sigma_t$ , and the fracture energy,  $G_F$ , being estimated according to Model Code<sup>29</sup> and Equation (1), respectively. The crushing energy,  $G_c$ , is calculated by means of Equation (3). Concerning the steel-bar reinforcement, the yield strength  $\sigma_y = 500$  MPa has been considered, and the reinforcement layer has been positioned in order to keep  $d/h = 0.9$ . All the investigated beams have a web thickness,  $b_w$ , and a flange thickness equal to  $h/4$  with a flange

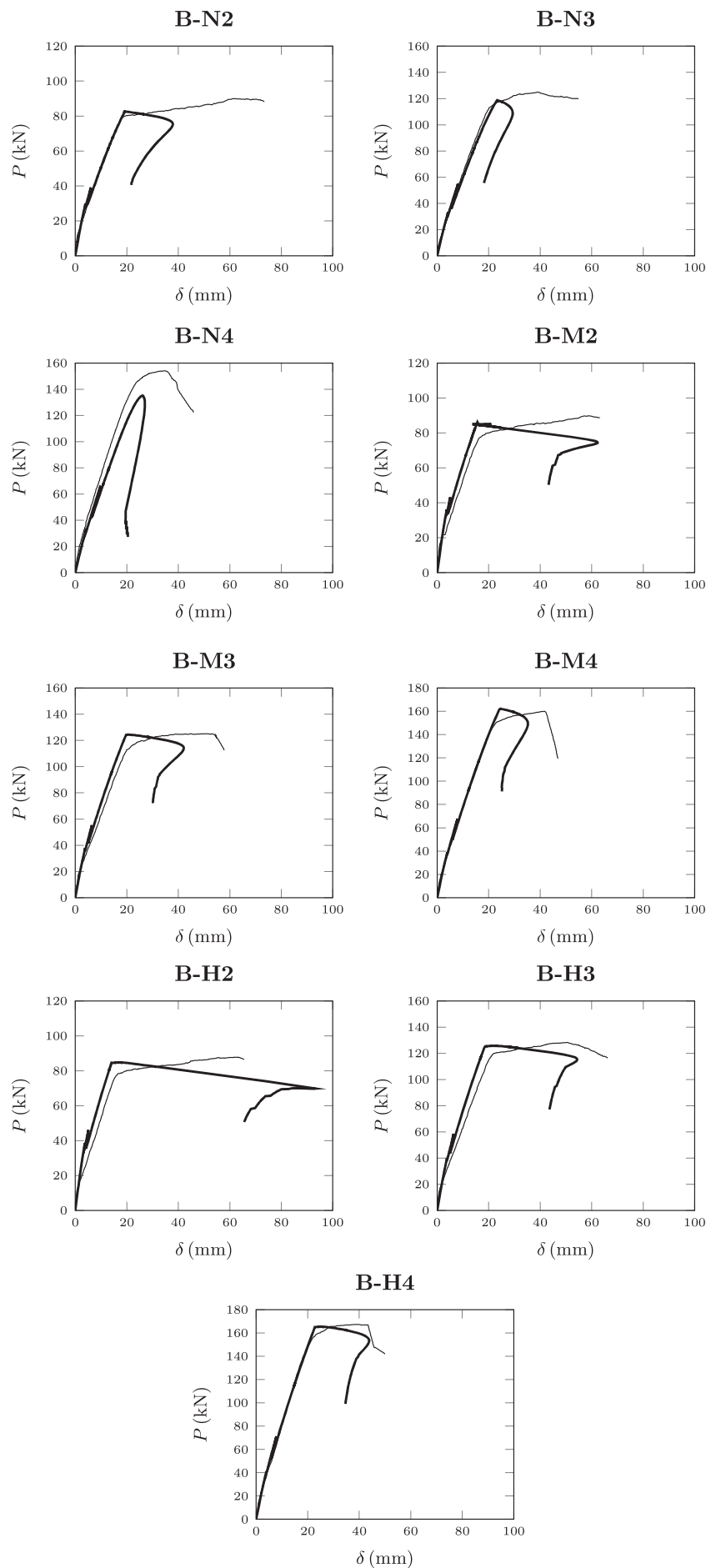


**FIGURE 11** Numerical (thick) versus experimental (thin) curves.

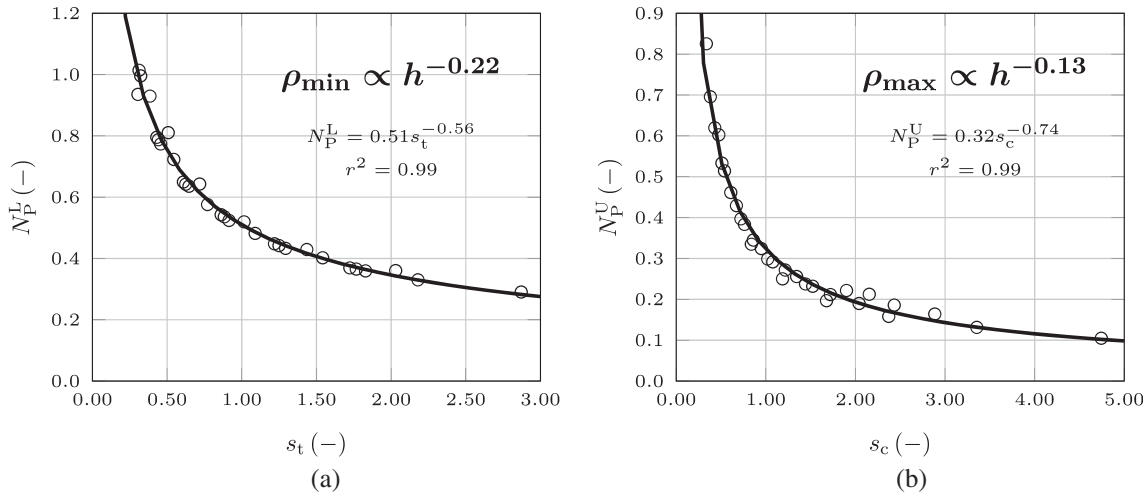


FIGURE 12 Ductile-to-brittle transitions in RC T-beams: (a)  $s_t$ - $N_P^L$ , and (b)  $s_c$ - $N_P^U$  best fit.

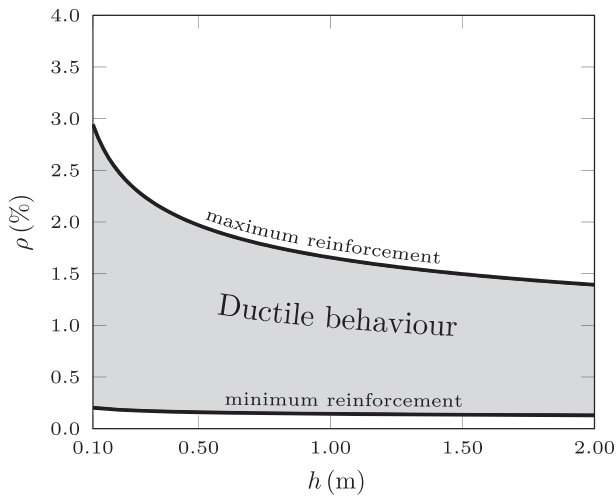


FIGURE 13 Upper and lower bounds for reinforcement ratio.

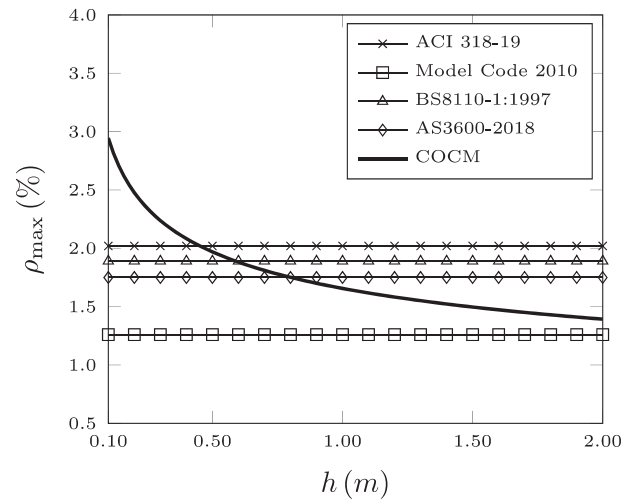


FIGURE 14 Comparison between different maximum reinforcement provisions.

width of  $4b_w$  (Figure 7a), whereas the beam depth,  $h$ , varies between 0.1 m and 3.2 m. For each beam depth, the reinforcement ratio has been changed iteratively in order to obtain an ultimate bending moment equal to the cracking bending moment for the estimation of the minimum reinforcement ratio,  $\rho_{\min}$ . Similarly, the maximum reinforcement ratio,  $\rho_{\max}$ , has been estimated as the reinforcement ratio beyond which concrete crushing precedes steel yielding. The results of the parametric study and the best-fitting relations in the planes  $s_t$ - $N_P^L$  and  $s_c$ - $N_P^U$  are reported in Figure 12.

From Figure 12a, we can find:

$$N_P^L = 0.51 s_t^{-0.56} \quad (17)$$

Considering the definition of  $N_P^L$  and  $s_t$ , we have:

$$\rho_{\min} = 0.51 \frac{\sigma_t^{0.56} K_{IC}^{0.44}}{\sigma_y h^{0.22}} \quad (18)$$

where a scale effect on the minimum reinforcement percentage is found to be  $h^{-0.22}$ .

On the other hand, in Figure 12b the results of the parametric analysis regarding the maximum reinforcement ratio,  $\rho_{\max}$ , leads to:

$$N_P^U = 0.32 s_c^{-0.74} \quad (19)$$

Considering the definitions of  $N_P^U$  and  $s_c$ , it is possible to find:

$$\rho_{\max} = 0.32 \frac{\sigma_c^{0.74} (\sqrt{G_c E})^{0.26}}{\sigma_y h^{0.13}} \quad (20)$$

where the scale effect on the maximum reinforcement percentage is found to be  $h^{-0.13}$ .

In this context, it is interesting to recall that previous analyses of RC rectangular cross-sections<sup>24,48,49,61</sup> provided a scale effect on the minimum reinforcement percentage proportional to  $h^{-0.15}$ , and a scale effect on the maximum reinforcement percentage proportional to  $h^{-0.25}$ , thus defining an effective range in which structures can develop a safe ductile behavior at ULS (Figure 13). Current Standards, such as Model Code,<sup>29</sup> BS 81110,<sup>62</sup> AS 3600,<sup>63</sup> and ACI,<sup>57</sup> completely disregard the size-scale effects on these two reinforcement percentages leading to a wrong assessment of the rotation capacity of real structures.<sup>64</sup> The provisions imposed by Standards together with the scale-dependent maximum reinforcement percentage provided by the Cohesive/Overlapping Crack Model are reported in Figure 14, suggesting that current Standards are not able to fully ensure RC safety.

In the case of T-beams having flange/web ratio equal to 4, a consistent variation in the power-law exponents is found, suggesting that the beam cross-section shape can have significant effects on the ductile-to-brittle transitions occurring in RC.

## 6 | CONCLUSIONS

In the present paper, by means of the Cohesive/Overlapping Crack Model (COCM), an effective estimation of the minimum reinforcement percentage for RC T-beams is performed, emphasizing its  $h^{-0.22}$  power-law scale dependence, where  $h$  is the beam depth. In addition, numerical studies are carried out in order to confirm how the extension of the plastic plateau developing after steel yielding is inversely proportional to beam depth,  $h$ , and reinforcement ratio,  $\rho$ . This evidence is accompanied by an analogous existence of a scale-dependent maximum reinforcement percentage for RC T-beams with a  $h^{-0.13}$  power-law beyond which the structure is unable to develop any ductility due to concrete crushing occurring prior to steel yielding. In the case of the upper bound, not only economical but also safety reasons justify the present study.

For PC beams and high-performance concrete, the application of the COCM demonstrates how these structures exhibit a more brittle behavior due to the presence of the prestressing force and/or the high strength of the concrete matrix.

## NOTATION

$\ell$	beam span
$\vartheta$	cross-section local rotation
$[K_F]$	matrix of nodal displacements generated by unit forces


$\{F\}$	vector of nodal forces
$\{F_p\}$	vector of nodal forces generated by the prestressing force
$\{K_M\}$	vector of nodal displacements generated by unit bending moment
$\{w\}$	vector of nodal displacements
$A_s$	steel area
$A_{sp}$	prestressed steel area
$b$	beam thickness
$b_w$	beam web thickness
$d$	beam effective depth
$F_p$	prestressing force
$F_y$	steel yield force
$G_c$	crushing energy
$G_F$	fracture energy
$h$	beam depth
$M$	bending moment
$N_P^L$	lower bound reinforcement brittleness number
$N_P^U$	upper bound reinforcement brittleness number
$P$	applied load
$s_c$	compression matrix brittleness number
$s_t$	tension matrix brittleness number
$w^c$	fictitious interpenetration
$w_{cr}^c$	critical value of the fictitious interpenetration
$w^t$	crack opening displacement
$w_{cr}^t$	critical value of the crack opening displacement
$w_y^t$	steel-bar yielding crack opening displacement
$\delta$	beam mid-span deflection
$\varepsilon_c$	concrete ultimate compression strain
$\varepsilon_t$	concrete ultimate tension strain
$\rho$	reinforcement percentage ( $A_s/b_w h$ )
$\rho_{max}$	maximum reinforcement percentage
$\rho_{min}$	minimum reinforcement percentage
$\rho_p$	prestressing reinforcement percentage ( $A_{sp}/b_w h$ )
$\sigma_c$	concrete compression strength
$\sigma_t$	concrete tension strength
$\sigma_y$	steel-bar yield strength

## DATA AVAILABILITY STATEMENT

The data that support the findings of this study are available from the corresponding author upon reasonable request.

## ORCID

Renato Cafarelli  <https://orcid.org/0000-0003-2076-1053>

Federico Accornero  <https://orcid.org/0000-0002-9638-8411>

## REFERENCES

1. von Kármán T, Tsien HS. The buckling of thin cylindrical shells under axial compression. *J Aeronaut Sci.* 1941;8:303–12. <https://doi.org/10.2514/8.10722>

2. Carlson RL, Sendelbeck RL, Hoff NJ. Experimental studies of the buckling of complete spherical shells. *Exp Mech*. 1967;7: 281–8. <https://doi.org/10.1007/BF02327133>
3. Kaplan A. Buckling of spherical shells. Thin Shell structures: theory, experiment and design. Englewood Cliffs, NJ: Prentice Hall; 1974. p. 247–88.
4. Zhu W, Bartos PJM. “Effects of combined fiber treatments and matrix modifications on toughness of aged GRC”, Proceedings of the 9<sup>th</sup> Congress of the GRCA, Wigan, UK. 1993.
5. Carpinteri A. “A fracture mechanics model for reinforced concrete collapse”, Proceedings of the IABSE Colloquium On Advanced Mechanics Of Reinforced Concrete, Delft, Netherlands. 1981.
6. Carpinteri A. Stability of fracturing process in RC beams. *J Struct Eng (ASCE)*. 1984;110:544–58. [https://doi.org/10.1061/\(ASCE\)0733-9445\(1984\)110:3\(544\)](https://doi.org/10.1061/(ASCE)0733-9445(1984)110:3(544))
7. Carpinteri A, Accornero F. The bridged crack model with multiple fibres: local instabilities, scale effects, plastic shake-down, and hysteresis. *Theor Appl Fract Mech*. 2019;104:102351. <https://doi.org/10.1016/j.tafmec.2019.102351>
8. Carpinteri A. Static and energetic fracture parameters for rocks and concretes. *Constr Build Mater (RILEM)*. 1981:151–62. <https://doi.org/10.1007/BF02473919>
9. Carpinteri A. Interpretation of the Griffith instability as a bifurcation of the global equilibrium. Proceedings of the NATO advanced research workshop on application of fracture mechanics to cementitious composites. Dordrecht, Netherlands: Martinus Nijhoff Publishers; 1985. p. 287–316. [https://doi.org/10.1007/978-94-009-5121-1\\_10](https://doi.org/10.1007/978-94-009-5121-1_10)
10. Carpinteri A. Cusp catastrophe interpretation of fracture instability. *J Mech Phys Solids*. 1989;37:567–82. [https://doi.org/10.1016/0022-5096\(89\)90029-X](https://doi.org/10.1016/0022-5096(89)90029-X)
11. fib Bulletin 242. Ductility of reinforced concrete structures. Stuttgart (Germany): Sprint-Druck; 1998.
12. Cohn MZ. Inelasticity of reinforced concrete and structural standards. *J Struct Div (ASCE)*. 1979;105:2221–41. <https://doi.org/10.1061/JSDEAG.0005274>
13. Siviero E. Rotation capacity of nondimensional members in structural concrete. CEB bulletin d'Information No. 105. Lusanne: Comité Euro-International du Béton; 1976. p. 206–22.
14. Eifler H, Plauk G. Drehfähigkeit plastischer Gelenke in biegebeanspruchten Stahlbetonkonstruktionen. Bericht der Bundesanstalt für Materialprüfung (BAM) zum Forschungsvorhaben BAM. Berlin: IRB-Verlag; 1974.
15. Mattock AH. Rotational capacity of hinging regions in reinforced concrete beams. Flexural mechanics of reinforced concrete. Miami (USA): ASCE-ACI International Symposium; 1965. p. 143–81.
16. Corley WG. Rotational capacity of reinforced concrete beams. *J Struct Div (ASCE)*. 1966;95:122–46. <https://doi.org/10.1061/JSDEAG.0001504>
17. Markeset G. “Failure of concrete under compressive strain gradients”, PhD Thesis, 1993, The Norwegian Institute of Technology, Trondheim (Norway).
18. Bigaj AJ. “Structural dependence of rotation capacity of plastic hinges in RC beams and slabs”, PhD Thesis, 1999, Delft University of Technology, Delft (Netherlands).
19. Hillerborg A. Fracture mechanics concepts applied to moment capacity and rotational capacity of reinforced concrete beams. *Eng Frac Mech*. 1990;35:233–40. [https://doi.org/10.1016/0013-7944\(90\)90201-Q](https://doi.org/10.1016/0013-7944(90)90201-Q)
20. Cosenza E, Greco C, Manfredi G. Theoretical evaluation of inelastic rotations and displacements in the reinforced concrete monodimensional elements (in Italian). *Atti dell'Accademia Nazionale Dei Lincei*. 1991;2:249–58.
21. Cosenza E, Greco C, Manfredi G. Evaluation of plastic rotations in r.c. beams: comparison between theoretical and experimental results. Istituto di Ingegneria Civile. Salerno: Università di Salerno (Italy); 1992.
22. Bigaj AJ. “Size effects on rotational capacity of plastic hinges in reinforced concrete beams”, Progress in concrete research. Vol 3. Delft (Netherlands): Delft University of Technology; 1992.
23. Bigaj AJ, Walraven J. Size effects in plastic hinges of reinforced concrete members. *Heron*. 2002;47:53–75.
24. Carpinteri A, Corrado M. Upper and lower bounds for structural design of RC members with ductile response. *Eng Struct*. 2011;33:3432–41. <https://doi.org/10.1016/j.engstruct.2011.07.007>
25. Barenblatt GI. “Scaling”, Cambridge texts in applied mathematics. Cambridge: Cambridge University Press; 2003.
26. Carpinteri A, Accornero F. Dimensional analysis of critical phenomena: self-weight failure, turbulence, resonance, fracture. *Phys Mesomech*. 2021;24:459–63. <https://doi.org/10.1134/S102995992104010X>
27. Hillerborg A, Modéer M, Petersson P-E. Analysis of crack formation and crack growth in concrete by means of fracture mechanics and finite elements. *Cem Concr Res*. 1976;6:773–81. [https://doi.org/10.1016/0008-8846\(76\)90007-7](https://doi.org/10.1016/0008-8846(76)90007-7)
28. Petersson P-E. “Crack growth and development of fracture zones in plain concrete and similar materials”, PhD Thesis, 1981, Lund University, Sweden.
29. fib (Fédération Internationale du Béton). Model Code for Concrete Structures 2010. New York, New York, USA: John Wiley & Sons; 2013.
30. Ruiz G, Elices M, Planas J. Size effect and bond-slip dependence of lightly reinforced concrete beams. Minimum reinforcement in concrete members. Oxford, UK: Elsevier; 1999. p. 67–97.
31. Belgin CM, Sener S. Size effect on failure of overreinforced concrete beams. *Eng Frac Mech*. 2008;75:2308–19. <https://doi.org/10.1016/j.engfracmech.2007.09.006>
32. Hognestad E. A study of combined bending and axial load in reinforced concrete members. Univ Illinois Eng Exp Station. 1951; 49:399.
33. Popovic S. A numerical approach to the complete stress-strain curve of concrete. *Cem Concr Res*. 1973;3:583–99. [https://doi.org/10.1016/0008-8846\(73\)90096-3](https://doi.org/10.1016/0008-8846(73)90096-3)
34. Meyer J. “Ein Beitrag zur untersuchung der verformungsfähigkeit von bauteilen aus beton unter biegendruckbeanspruchung”, PhD Thesis (in German), 1998, Institut für Massivbau und Baustofftechnologie. 1998.
35. Carrasquillo RL, Nilson AH, Slate FO. Properties of high strength concrete subjected to short-term loads. *ACI Struct J*. 1981;78:171–8. <https://doi.org/10.14359/6914>
36. Shah SP, Gokoz U, Ansari F. An experimental technique for obtaining complete stress-strain curves for high strength concrete. *Cement Concr Aggregate*. 1981;3:21–7. <https://doi.org/10.1520/CCA10198J>



37. Kotsovos MD. Effect of testing techniques on the post-ultimate behaviour of concrete in compression. *Matériaux et Construction (RILEM)*. 1983;16:3–12. <https://doi.org/10.1007/BF02474861>
38. Torrenti JM, Benaija EH, Boulay C. Influence of boundary conditions on strain softening in concrete compression test. *J Eng Mech*. 1993;119:2369–84. [https://doi.org/10.1061/\(ASCE\)0733-9399\(1993\)119:12\(2369\)](https://doi.org/10.1061/(ASCE)0733-9399(1993)119:12(2369))
39. van Vliet MRA, van Mier JGM. Experimental investigation of concrete fracture under uniaxial compression. *Mech Cohes Frictional Mater*. 1996;1:115–27. [https://doi.org/10.1002/\(SICI\)1099-1484\(199601\)1:1<115::AID-CFM6>3.0.CO;2-U](https://doi.org/10.1002/(SICI)1099-1484(199601)1:1<115::AID-CFM6>3.0.CO;2-U)
40. van Mier JGM, Shah SP, Arnaud M, Balayssac JP, Bascoul A, Choi S, et al. “Strain-softening of concrete in uniaxial compression”, report of the round Robin test carried out by RILEM TC 148-SCC. *Materials and Structures*. 1997;30:195–209. <https://doi.org/10.1007/BF02486177>
41. Jansen DC, Shah SP. Effect of length on compressive strain softening of concrete. *J Eng Mech*. 1997;123:25–35. [https://doi.org/10.1061/\(ASCE\)0733-9399\(1997\)123:1\(25\)](https://doi.org/10.1061/(ASCE)0733-9399(1997)123:1(25))
42. Del Viso JR, Carmona JR, Ruiz G. Shape and size effects on the compressive strength of high strength concrete. *Cem Concr Res*. 2008;38:386–95. <https://doi.org/10.1016/j.cemconres.2007.09.020>
43. Rokugo K, Koyanagi W. Role of compressive fracture energy of concrete on the failure behavior of reinforced concrete beams. *Applications of fracture mechanics to reinforced concrete*. New York, N.Y: Elsevier Applied Science; 1994. p. 437–64.
44. Markeset G, Hillerborg A. Softening of concrete in compression–localization and size effects. *Cement Concr Res*. 1995;25:702–8. [https://doi.org/10.1016/0008-8846\(95\)00059-L](https://doi.org/10.1016/0008-8846(95)00059-L)
45. Carpinteri A, Corrado M, Mancini G, Paggi M. The overlapping crack model for uniaxial and eccentric concrete compression tests. *Mag Concr Res*. 2009;61:745–57. <https://doi.org/10.1680/macr.2008.61.9.745>
46. Suzuki M, Akiyama M, Matsuzaki H, Dang TH. Concentric loading test of RC columns with normal and high-strength materials and averaged stress-strain model for confined concrete considering compressive fracture energy. *Proceedings of the Second International fib Congress*. Naples, Italy: Doppiavoce; 2006.
47. Carpinteri A, Corrado M, Paggi M, Mancini G. New model for the analysis of size-scale effects on the ductility of reinforced concrete elements in bending. *J Eng Mech*. 2009;135:221–9. [https://doi.org/10.1061/\(ASCE\)0733-9399\(2009\)135:3\(221\)](https://doi.org/10.1061/(ASCE)0733-9399(2009)135:3(221))
48. Accornero F, Cafarelli R, Carpinteri A. The cohesive/overlapping crack model for plain and reinforced concrete beams: scale effects on cracking and crushing failure. *Mag Concr Res*. 2022;74:433–50. <https://doi.org/10.1680/jmacr.20.00260>
49. Carpinteri A, Accornero F, Cafarelli R. Scale-dependent maximum reinforcement percentage in reinforced concrete beams. *Struct Concr (Fib)*. 2021;22:2155–66. <https://doi.org/10.1002/suco.202000573>
50. Rüsch H. Researches toward a general flexural theory for structural concrete. *ACI Struct J*. 1960;57:1–28. <https://doi.org/10.14359/8009>
51. Mattock AH, Kriz LB. Ultimate strength of nonrectangular structural concrete members. *ACI Struct J*. 1961;57:737–66. <https://doi.org/10.14359/8044>
52. Sturman GM, Shah SP, Winter G. Effects of flexural strain gradients on microcracking and stress-strain behavior of concrete. *ACI Struct J*. 1965;62:805–22. <https://doi.org/10.14359/7725>
53. Ibrahim HHH, Mac Gregor JG. Modification of the ACI rectangular stress block for high-strength concrete. *ACI Struct J*. 1997;94:40–8. <https://doi.org/10.14359/459>
54. Feenstra PH, de Borst R. Constitutive model for reinforced concrete. *J Eng Mech (ASCE)*. 1995;121:587–95. [https://doi.org/10.1061/\(ASCE\)0733-9399\(1995\)121:5\(587\)](https://doi.org/10.1061/(ASCE)0733-9399(1995)121:5(587))
55. Accornero F, Cafarelli R, Carpinteri A. Cracking and crushing in prestressed concrete beams. *ACI Struct J*. 2021;118:101–9. <https://doi.org/10.14359/51728184>
56. Branson DE. Instantaneous and time-dependent deflections of simple and continuous reinforced concrete beams. *Alabama Highway Department*. 1963;7:1–78.
57. ACI (American Concrete Institute). *ACI 318–19: building code requirements for structural concrete*. MI, USA: American Concrete Institute, Farmington Hills; 2019.
58. ACI (American Concrete Institute). *ACI reinforced concrete design handbook*. Vol 2. MI, USA: American Concrete Institute, Farmington Hills; 2021.
59. Ashour SA. Effect of compressive strength and tensile reinforcement ratio on flexural behaviour of high-strength concrete beams. *Eng Struct*. 2000;22:413–23. [https://doi.org/10.1016/S0141-0296\(98\)00135-7](https://doi.org/10.1016/S0141-0296(98)00135-7)
60. AASHTO. *LRFD minimum flexural reinforcement requirements*. National Cooperative Highway Research Program (NCHRP). Res Report. 2019;906.
61. Carpinteri A, Accornero F, Cafarelli R. Scale effects in prestressed concrete structures: maximum reinforcement percentage to avoid brittle crushing. *Eng Struct*. 2022;255:113911. <https://doi.org/10.1016/j.engstruct.2022.113911>
62. BS8110-1. *Code of practice for design and construction*. Structural use of concrete–Part 1. London, UK: BSI; 1997.
63. AS 3600 (Standards Australia). *Concrete Structures*, Standards Australia, Sydney, Australia. 2018.
64. Naaman AE. Limits of reinforcement in 2002 ACI code: transitions, flaws, and solutions. *ACI Struct J*. 2004;101:209–18. <https://doi.org/10.14359/13018>

## AUTHOR BIOGRAPHIES

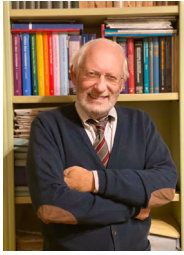


**Renato Cafarelli**, DISEG, Politecnico di Torino, Turin, Italy.



**Federico Accornero**, Associate Professor of Structural Mechanics, College of Engineering, Shantou University, Shantou, China.





**Alberto Carpinteri**, Chair Professor of Structural Mechanics, DISEG, Politecnico di Torino, Turin, Italy; Zhujiang (Pearl River) Professor of Guangdong Province, College of Engineering, Shantou University, Shantou, China.

**How to cite this article:** Cafarelli R, Accornero F, Carpinteri A. Size-scale effects in high-performance reinforced and prestressed concrete T-beams. *Structural Concrete*. 2023. <https://doi.org/10.1002/suco.202200673>